Letter

Manipulation of magnetic topological textures via perpendicular strain and polarization in van der Waals magnetoelectric heterostructures

Zhong Shen, Shuai Dong,[*] and Xiaoyan Yao[†]

Key Laboratory of Quantum Materials and Devices of Ministry of Education, School of Physics,
Southeast University, Nanjing 211189, China

The multifunctional manipulation of magnetic topological textures such as skyrmions and bimerons in energy-efficient ways is of great importance for spintronic applications, but it is still a big challenge. Here, by first-principles calculations and atomistic simulations, the creation and annihilation of skyrmions/bimerons, as key operations for the reading and writing of information in spintronic devices, are achieved in a van der Waals magnetoelectric CrISe/In$_2$Se$_3$ heterostructure via perpendicular strain or electric field without an external magnetic field. In addition, bimeron-skyrmion conversion, size modulation, and reversible magnetization switching from in plane to out of plane could also be realized in magnetic-field-free ways. Moreover, the topological charge and morphology can be precisely controlled by a small magnetic field. The strong Dzyaloshinskii-Moriya interaction and tunable magnetic anisotropy energy in a wide window are found to play vital roles in such energy-efficient multifunctional manipulation, and the underlying physical mechanisms are elucidated. Our work predicts the CrISe/In$_2$Se$_3$ heterostructure to be an ideal platform to address this challenge in spintronic applications, and theoretically guides the low-dissipation multifunctional manipulation of magnetic topological textures.

Introduction. Magnetic skyrmions are topologically protected spin textures with high stability against defects and disorder [1–4]. Since the first experimental observation in 2009 [5], skyrmions have been investigated intensively both experimentally [6–11] and theoretically [12–20] due to their promising applications in next-generation nonvolatile spintronic devices with high storage density and low-energy dissipation. As the counterpart of skyrmions in easy-plane magnets, bimerons [21–23] can also be used as information carriers for memory devices. Two key parameters for the stability of skyrmions and bimerons are the Dzyaloshinskii-Moriya interaction (DMI) [24,25] and magnetic anisotropy, both of which originate from spin-orbit coupling.

For practical applications, it is extremely important to manipulate the size and morphology of the topological textures, and to control their generation and annihilation in a convenient and low-dissipation way. Compared to the widely used traditional methods with energy dissipation, such as spin-polarized currents [26–28], thermal excitation [29,30], and an external magnetic field pulse [31,32], strain [33,34] and electric fields [22,35–37] are more energy-efficient ways to tune magnetism. Recent works have demonstrated the creation and annihilation of bimerons [21] as well as the conversion from loops of vortices and antivortices to skyrmions [35], both of which are induced by a change of magnetic anisotropy

energy (MAE). However, in the above works, the MAE jumps between specific values, rather than changing nearly continuously in a wide range, which limits further regulations of skyrmions and bimerons. Thus, the multifunctional manipulation of magnetic topological textures remains to be investigated and potential magnetoelectric systems are yet to be discovered.

Here, by first-principles calculations and atomistic simulations, we theoretically demonstrate the multifunctional manipulation of magnetic skyrmions and bimerons in a van der Waals magnetoelectric heterostructure CrISe/In$_2$Se$_3$. Generation and annihilation, size modulation, and bimeron-skyrmion conversion could all be realized by applying perpendicular strain or electric field without any external magnetic field. The MAE, which is tunable in a wide range from −3.5 to 1.6 meV, namely the anisotropy switchable from easy plane (in plane) to easy axis (out of plane), is found to play a crucial role in this multifunctional manipulation of skyrmions and bimerons.

Methods. First-principles calculations are carried out by using the Vienna *ab initio* simulation package (VASP) [38] based on density functional theory (DFT). The phonon band structures are calculated by using the PHONOPY code [39,40] with a $3 \times 3 \times 1$ supercell to confirm the dynamic stability of CrISe. The visualization of crystal structures is realized by VESTA [41]. To explore the topological magnetic textures of CrISe/In$_2$Se$_3$, we perform atomistic simulations based on the Heisenberg model and Landau-Lifshitz-Gilbert (LLG) equation [42,43] as implemented in the SPIRIT package [44]. See Supplemental Material [45] for more details.

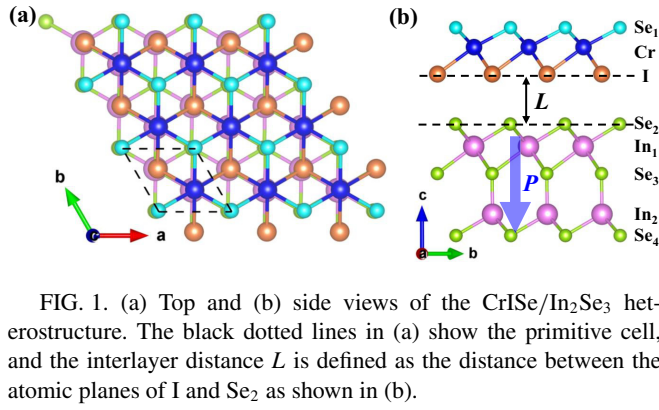[*]sdong@seu.edu.cn
[†]yaoxiaoyan@seu.edu.cn

FIG. 1. (a) Top and (b) side views of the CrISe/In$_2$Se$_3$ heterostructure. The black dotted lines in (a) show the primitive cell, and the interlayer distance L is defined as the distance between the atomic planes of I and Se$_2$ as shown in (b).

The magnetic properties of CrISe/In$_2$Se$_3$ are investigated based on the following Hamiltonian:

$$H = J_1 \sum_{\langle i,j \rangle} \vec{S}_i \cdot \vec{S}_j + J_2 \sum_{\langle\langle i,k \rangle\rangle} \vec{S}_i \cdot \vec{S}_k + J_3 \sum_{\langle\langle\langle i,l \rangle\rangle\rangle} \vec{S}_i \cdot \vec{S}_l$$
$$+ \sum_{\langle i,j \rangle} \vec{d}_{ij} \cdot (\vec{S}_i \times \vec{S}_j) + K \sum_i \left(S_i^z\right)^2$$
$$+ \mu_{Cr} \sum_i \vec{B} \cdot \vec{S}_i. \qquad (1)$$

Here, the first three terms describe the isotropic Heisenberg exchanges with J_1, J_2, J_3 being the exchange coefficients between the nearest-neighbor (NN), second NN, and third NN Cr atoms. $\vec{S}_i$ is a unit vector representing the orientation of the spin at the ith Cr atom. The DMI, magnetic anisotropy, and external magnetic field are characterized by the parameters $\vec{d}_{ij}$, K, and $\vec{B}$, respectively. μ_{Cr} is the magnetic moment of Cr atoms. All the magnetic parameters are extracted from the energy differences of distinct magnetic configurations (see Supplemental Material [45] for more details).

Results and discussion. The In$_2$Se$_3$ monolayer is a room-temperature ferroelectric material with reversible spontaneous electric polarization [46,47]. The CrISe monolayer is predicted to be a room-temperature ferromagnetic semiconductor with intrinsic broken inversion symmetry due to the Janus structure [20]. The dynamical stability of the CrISe monolayer is verified by the phonon spectrum calculation in Fig. S3(c) [45]. Considering that van der Waals (vdW) monolayers are easy to stack together, many two-dimensional (2D) vdW heterostructures have been experimentally synthesized, such as MoS$_2$/In$_2$Se$_3$ [48], WSe$_2$/In$_2$Se$_3$ [49], and FePS$_3$/Fe$_3$GeTe$_2$ [50]. Here, we construct the CrISe/In$_2$Se$_3$ heterostructure with the ferroelectric polarization (P) of In$_2$Se$_3$ fixed along the $-Z$ direction. The lattice mismatch is no more than 4% for both CrISe and In$_2$Se$_3$ layers with optimized lattice constants of 3.948 Å for the CrISe/In$_2$Se$_3$ heterostructure. Figures 1(a) and 1(b) show the top and side views of the CrISe/In$_2$Se$_3$ heterostructure in the most stable stacking mode (see Supplemental Material for more details [45]). The magnetic atoms Cr form a triangular lattice with a calculated magnetic moment about 3 μ_B per Cr. Then, the distance between the atomic layers of I and Se$_2$ is defined to be the interlayer distance L as indicated in Fig. 1(b). The weak vdW interaction between CrISe and In$_2$Se$_3$ layers
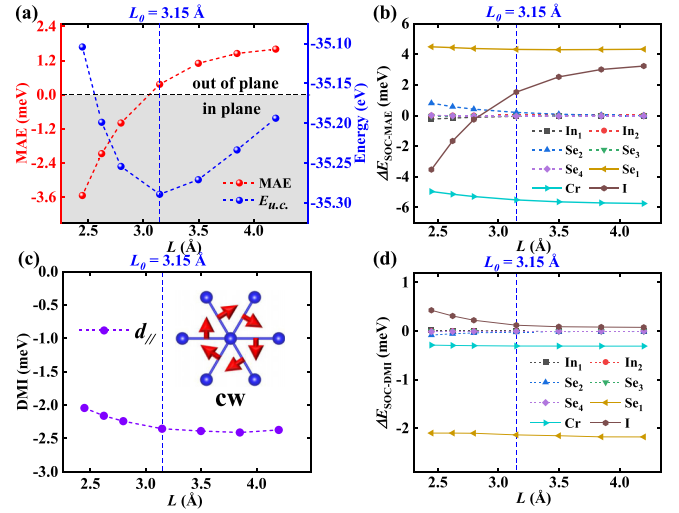

FIG. 2. (a) MAE and the energy of the unit cell ($E_{u.c.}$), (b) atom-resolved SOC energy associated with MAE ($\Delta E_{SOC\text{-}MAE}$), (c) DMI, and (d) atom-resolved SOC energy associated with DMI ($\Delta E_{SOC\text{-}DMI}$) as functions of the interlayer distance L. The optimal interlayer distance $L_0 = 3.15$ Å is indicated by blue dotted lines in (a)–(d). The inset of (c) demonstrates the in-plane components of DMI between the nearest-neighboring Cr atoms.

provides convenience for exerting strain vertically, which can be achieved in first-principles calculations by changing the interlayer distance L [51,52]. According to the force acting on atoms I and Se$_2$, we estimate that the necessary pressure for the manipulation of skyrmions and bimerons is in the range of −1.1 to 2.7 GPa.

We first focus on the magnetic anisotropy energy (MAE) of the CrISe/In$_2$Se$_3$ heterostructure. According to the Mermin-Wagner theorem [53], long-range magnetic order is absent in a 2D isotropic Heisenberg system with short-range interactions. However, this restriction can be removed by the spin-exchange interactions [54] and MAE [55–57] in finite-size 2D vdW magnets. Here, MAE is defined as the energy difference between the in-plane (E_x) and the out-of-plane (E_z) ferromagnetic states: MAE $= E_x - E_z$. Thus, a positive (negative) MAE corresponds to the easy-axis (easy-plane) anisotropy. As shown in Fig. 2(a), the optimal interlayer distance of CrISe/In$_2$Se$_3$ is $L_0 = 3.15$ Å at which the energy of the unit cell ($E_{u.c.}$) is lowest. Meanwhile, the MAE of intrinsic CrISe/In$_2$Se$_3$ is 0.4 meV per unit cell with the magnetic easy axis being out of plane. The MAE can be enhanced up to 1.6 meV with increased L. Interestingly, as L is reduced, the easy-axis anisotropy switches to easy plane and the MAE can be further tuned to −3.5 meV. This means that magnetization switching, which is an important operation in spintronic devices especially for the writing operation, can be achieved by tuning perpendicular strain. In addition, it is noteworthy that the switchable magnetic anisotropy between easy axis and easy plane provides the possibility not only for the existence of both skyrmions and bimerons in CrISe/In$_2$Se$_3$ but also for a controllable conversion between them. Figure 2(b) shows the atom-resolved SOC energy associated with MAE ($\Delta E_{SOC\text{-}MAE}$), from which we can see that the L-dependent MAE and the switch of magnetic anisotropy are dominated

by I atoms. The Cr and Se_1 atoms in the CrISe layer also have significant contributions to MAE. However, they are far away from the ferroelectric In_2Se_3 layer, and thus their contributions to MAE are hardly affected by L. The mechanism of the drastically changed MAE contribution from I atoms can be further elucidated microscopically by the L-dependent hybridization of the I-$3p$ orbitals according to the second-order perturbation theory [58,59] (see Supplemental Material for more details [45]).

The stability of topological spin textures, such as skyrmions and bimerons, is closely related to the Dzyaloshinskii-Moriya interaction (DMI), which stems from SOC and broken spatial inversion symmetry. To realize nanoscale skyrmions and bimerons, great effort has been made in finding materials with large DMI both experimentally [60–62] and theoretically [19,63–66]. According to Moriya's rule [25], since a mirror plane perpendicular to the bond between adjacent Cr atoms passes through the middle of this bond, the DMI between nearest-neighboring Cr is perpendicular to their bond. The DMI vector can be expressed as $\vec{d}_{ij} = d_{\parallel}(\vec{u}_{ij} \times \vec{z}) + d_z\vec{z}$. Here, $\vec{u}_{ij}$ and $\vec{z}$ are the unit vectors from site i to site j and along the z direction, respectively. The influence of d_z is negligible due to its vanishing contribution on average [65,67]. Thus we focus on the $d_{\parallel}$ in the following discussion. As seen in Fig. 2(c), a significant $d_{\parallel}$ of -2.35 meV is found in intrinsic $CrISe/In_2Se_3$, and its negative value means the clockwise chirality of the $d_{\parallel}$ direction denoted by red arrows in the inset. In addition, the $d_{\parallel}$ is almost unaffected by the change of L with the minimum value being -2.04 meV, which is stronger than those of VOI_2 (1.76 meV) [22] and $Cr_2I_3Cl_3$ (0.38 meV) [19]. Then, to clarify the microscopic origin of DMI, the $d_{\parallel}$ associated SOC energy $\Delta E_{SOC-DMI}$ [the energy difference between clockwise and anticlockwise spin configurations as shown in Figs. S5(a) and S5(b) of the Supplemental Material [45]] is calculated in Fig. 2(d). The dominant contribution to $d_{\parallel}$ mainly stems from the strong SOC of the heavy chalcogen atom Se_1. This is similar to the DMI in $MnXTe$ [65] and $CrXTe$ [68] monolayers which can be understood by the Fert-Levy mechanism [63,69]. The slightly reduced $d_{\parallel}$ with decreasing L is mainly caused by the increased $\Delta E_{SOC-DMI}$ of I with the opposite sign of that of Se_1.

To explore the topological spin textures in $CrISe/In_2Se_3$, atomistic simulations are performed with the magnetic parameters from first-principles calculations. As shown in Fig. 3(c), spontaneous skyrmions with diameters about 14 nm appear in intrinsic $CrISe/In_2Se_3$ without an external magnetic field. Then, the diameter of skyrmion can be tuned to sub-10 nm by a perpendicular stretch as indicated in Fig. 3(d). Figure 3(g) is the enlarged image of a Néel-type skyrmion with a small diameter of 8.0 nm. Notice that skyrmions in such a small size have been widely searched both theoretically and experimentally due to the promising application in low-energy consumption and high-density memory devices [11,70–73]. Then, as shown in Fig. 3(e), with a further increase of L, the skyrmions are annihilated to uniform ferromagnetic domains separated by Néel-type domain walls. More interestingly, as shown in Fig. 3(b), the magnetic-field-free conversion from skyrmions to bimerons is observed under
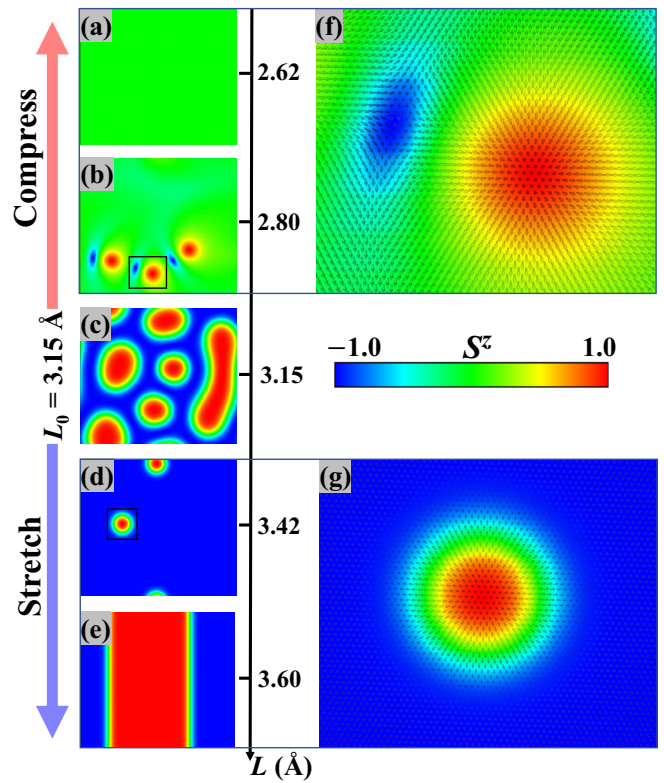

FIG. 3. (a)–(e) Magnetic-field-free spin textures of $CrISe/In_2Se_3$ heterostructure with different interlayer distances L. (f) and (g) enlarge the framed bimeron and skyrmion in (b) and (d).

perpendicular compression due to the switch of magnetic anisotropy from easy axis to easy plane, accompanied by the magnetization switching from out of plane to in plane. Figure 3(f) shows a zero-magnetic-field bimeron consisting of a meron ($Q = 0.5$) and an antimeron ($Q = 0.5$) with mutually reversed out-of-plane magnetizations. Here, Q is the topological charge defined as [15] $Q = \frac{1}{4\pi}\int \vec{S} \cdot (\partial_x\vec{S} \times \partial_y\vec{S})dxdy$. In addition, similar to the case of skyrmions, a size modulation of bimerons can be realized by further compression. Notice that, without rotational symmetry, bimerons are highly promising for racetrack applications. But so far, potential bimeron systems are much rarer than those of the skyrmions due to the exacting requirement of DMI [74,75] and the easy-axis magnetic anisotropy of most 2D vdW magnets [76–78]. Additionally, the bimerons in $CrISe/In_2Se_3$ may not only be produced, but also be annihilated to an in-plane ferromagnetic state by perpendicular compression as shown in Fig. 3(a). Thus, the minimum bits "1" and "0" for information storage can be achieved in $CrISe/In_2Se_3$ via the generation and annihilation of bimerons or skyrmions simply by a perpendicular strain without any external field. Notice that these metastable spin textures are not due to the frustration factor $|J_3/J_1|$ which is very small ($\sim$0.05), but due to the DMI and topological robustness of individual skyrmion or bimeron. We further calculate the energy difference between the spin textures in Fig. 3(b) [Fig. 3(d)] and the in-plane (out-of-plane) ferromagnetic state, which is 44 meV/spin (30 meV/spin).

The topological charge Q is a fingerprint for a topological property that determines the topologically protected stability,
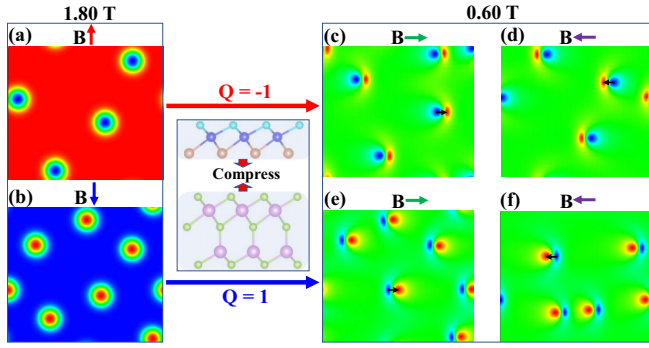
FIG. 4. Compression-induced conversion from skyrmions to bimerons with controllable topological charge and polarity. (a), (c), and (d) $Q = -1$, and (b), (e), and (f) $Q = 1$. The black arrows in (c)–(f) indicate the polarity of bimerons ($\vec{p}$), which is a unit vector from the center of spin down to the center of spin up. The color map is the same as that of Fig. 3.

FIG. 5. Regulation of MAE and magnetic topological textures by polarization. (a) MAE of the CrISe/In$_2$Se$_3$ heterostructure with opposite polarization of the In$_2$Se$_3$ layer as a function of interlayer distance L. (b) The enlarged range of L where the magnetic anisotropy can be tuned between the easy axis and easy plane by polarization. The round and square points in (b) correspond to the results by DFT and interpolation, respectively. (c)–(h) Magnetic-field-free spin textures of CrISe/In$_2$Se$_3$ with the polarization of In$_2$Se$_3$ along $+Z$ [(c)–(e)] and $-Z$ [(f)–(h)]. L are 2.63 Å [(c), (f)], 2.77 Å [(d), (g)], and 3.88 Å [(e), (h)], respectively. The color map of (c)–(h) is the same as that of Fig. 3.

and furthermore the other topology-related characteristics. For example, the sign and magnitude of the skyrmion Hall angle are directly related to Q [62,79]. Thus, the direction of lateral displacement in which a skyrmion deviates from the driving force can be controlled by restricting the sign of Q. Therefore, the control of Q plays an important role in the manipulation of topological textures, which can be realized in CrISe/In$_2$Se$_3$. As shown in Figs. 4(a) and 4(b), Q can be restricted as $+1$ (-1) with a magnetic field of 1.8 T along the $+Z$ $(-Z)$ direction. Then, by applying perpendicular compression and a small in-plane magnetic field of about 0.6 T, skyrmions transform into bimerons with Q unchanged. In addition, we define the polarity of the bimeron by a unit vector pointing from the spin-down center to the spin-up one as shown by the black arrows in Figs. 4(c)–4(f). It can be seen that the polarity vector of a bimeron is always in the same direction of the uniform background magnetization, which can be controlled by the direction of the external magnetic field. Notice that the speed of bimerons could be regulated by tuning the angle between the external drive and the background magnetization [79], which means the possibility to manipulate the polarity-related dynamic characteristics of a bimeron via an external magnetic field in similar magnetic systems. Therefore, a bimeron with a certain Q and polarity can be obtained in CrISe/In$_2$Se$_3$ by perpendicular strain and a magnetic field, which provides a superior platform for dynamic manipulation. In recent years, the manipulation of topological magnetic textures via an electric field has attracted considerable attention due to a nearly dissipation-free advantage [22,35]. Here, taking advantage of the reversible and nonvolatile ferroelectric polarization in the In$_2$Se$_3$ layer, the magnetic properties of the CrISe layer can be manipulated by an electric field in this heterostructure. The calculation indicates that CrISe/In$_2$Se$_3$ with the P of In$_2$Se$_3$ fixed along the $+Z$ direction ($P_\uparrow$) stabilizes in the same stacking mode as CrISe/In$_2$Se$_3$($P_\downarrow$). As shown in Fig. 5(a), as functions of interlayer distance L, the MAE of CrISe/In$_2$Se$_3$($P_\uparrow$) shows a similar trend as that of CrISe/In$_2$Se$_3$($P_\downarrow$), and the switch of magnetic anisotropy from easy axis to easy plane could be achieved in both cases. Interestingly, the change of MAE with L is not synchronous
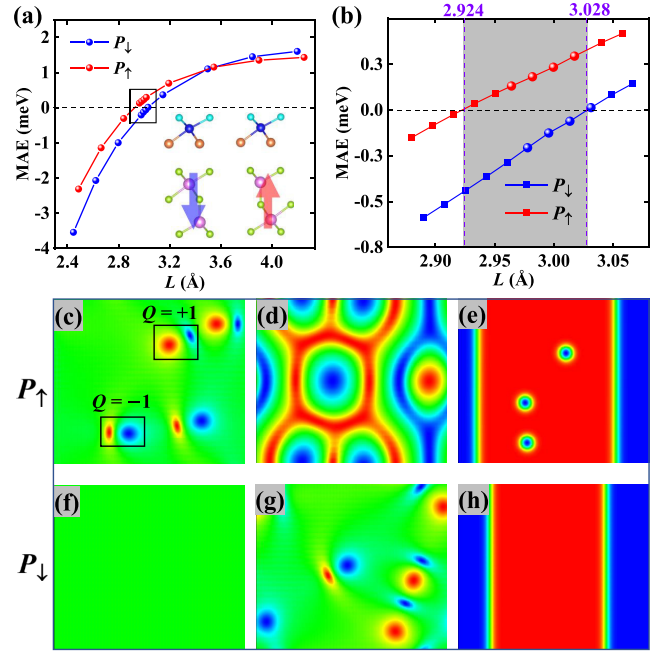
for CrISe/In$_2$Se$_3$($P_\uparrow$) and CrISe/In$_2$Se$_3$($P_\downarrow$), which enables us to tune the magnetic anisotropy and the topological spin textures via ferroelectric polarization. Figure 5(b) displays the details around MAE = 0 meV, from which we can see that in the shadow region (2.924 Å $< L <$ 3.028 Å), the magnetic anisotropy can be switched between easy axis and easy plane by tuning the polarization of In$_2$Se$_3$. In addition, as shown in Fig. 5(c) ($L = 2.63$ Å), bimerons with opposite Q's coexist in CrISe/In$_2$Se$_3$($P_\uparrow$) with an easy-plane magnetic anisotropy of -1.3 meV. Nevertheless, when the polarization of In$_2$Se$_3$ is reversed to the $P_\downarrow$ state, the bimerons disappear, accompanied by a vanishing Q [Fig. 5(f)]. When L increases to 2.77 Å, skyrmions with opposite Q's appear in CrISe/In$_2$Se$_3$($P_\uparrow$). Due to the weak easy-plane anisotropy (-0.6 meV), the in-plane magnetization part (green area) of skyrmions is wider than the skyrmions in easy-axis magnets. Similar spin textures are also demonstrated in MnBi$_2$Se$_2$Te$_2$/In$_2$Se$_3$ [35]. Then, by switching the polarization of In$_2$Se$_3$ to $P_\downarrow$, the easy-plane anisotropy is enhanced to -1.1 meV, resulting in the conversion from skyrmions to bimerons [Fig. 5(g)]. Moreover, with the L further increasing to 3.88 Å, the magnetic anisotropy transforms to an easy axis and sub-5-nm skyrmions appear in CrISe/In$_2$Se$_3$($P_\uparrow$), while the skyrmions are annihilated in CrISe/In$_2$Se$_3$($P_\downarrow$) due to the large MAE of 1.5 meV. Thus, we demonstrate that the creation and

annihilation of both skyrmions and bimerons, as well as the conversion between them can be realized in $CrISe/In_2Se_3$ by applying an electric field to reverse the ferroelectric polarization of In_2Se_3. Such magnetic-field-free multifunctional control of magnetic topological textures by polarization is highly desired in nonvolatile data storage with low-energy consumption.

Conclusion. In conclusion, by first-principles calculations and atomistic simulations, we predict a vdW magnetoelectric heterostructure $CrISe/In_2Se_3$ to be an ideal platform for magnetization switching and the multifunctional manipulation of magnetic topological textures in energy-efficient ways. By tuning perpendicular strain, the MAE can be tuned in a wide window from -3.5 to 1.6 meV, while the magnetic anisotropy can be switched between in plane and out of plane. Thereby,

the generation and annihilation of skyrmions and bimerons, the conversion between them, as well as the size modulation could all be manipulated in this magnetic-field-free way. Moreover, the multifunctional manipulation of skyrmions and bimerons can also be achieved by applying an electric field to tune the ferroelectric polarization of In_2Se_3. Our study predicts $CrISe/In_2Se_3$ as a promising candidate for spintronic applications, guiding the way for the low-dissipation manipulation of magnetic topological textures via strain and polarization.

[1] A. N. Bogdanov and D. A. Yablonskiǐ, Sov. Phys. JETP **68**, 101 (1989).

[2] A. Bogdanov and A. Hubert, J. Magn. Magn. Mater. **195**, 182 (1999).

[3] J. Sampaio, V. Cros, S. Rohart, A. Thiaville, and A. Fert, Nat. Nanotechnol. **8**, 839 (2013).

[4] J. Hagemeister, N. Romming, K. von Bergmann, E. Y. Vedmedenko, and R. Wiesendanger, Nat. Commun. **6**, 8455 (2015).

[5] S. Muhlbauer, B. Binz, F. Jonietz, C. Pfleiderer, A. Rosch, A. Neubauer, R. Georgii, and P. Boni, Science **323**, 915 (2009).

[6] J. Zhang, Y. Zhang, Y. Gao, G. Zhao, L. Qiu, K. Wang, P. Dou, W. Peng, Y. Zhuang, Y. Wu, G. Yu, Z. Zhu, Y. Zhao, Y. Guo, T. Zhu, J. Cai, B. Shen, and S. Wang, Adv. Mater. **32**, e1907452 (2020).

[7] Z. Hou, W. Ren, B. Ding, G. Xu, Y. Wang, B. Yang, Q. Zhang, Y. Zhang, E. Liu, F. Xu, W. Wang, G. Wu, X. Zhang, B. Shen, and Z. Zhang, Adv. Mater. **29**, 1701144 (2017).

[8] Z. Hou, Q. Zhang, X. Zhang, G. Xu, J. Xia, B. Ding, H. Li, S. Zhang, N. M. Batra, P. Costa, E. Liu, G. Wu, M. Ezawa, X. Liu, Y. Zhou, X. Zhang, and W. Wang, Adv. Mater. **32**, e1904815 (2020).

[9] K. Niitsu, Y. Liu, A. C. Booth, X. Yu, N. Mathur, M. J. Stolt, D. Shindo, S. Jin, J. Zang, N. Nagaosa, and Y. Tokura, Nat. Mater. **21**, 305 (2022).

[10] R. Brearton, L. A. Turnbull, J. A. T. Verezhak, G. Balakrishnan, P. D. Hatton, G. van der Laan, and T. Hesjedal, Nat. Commun. **12**, 2723 (2021).

[11] X. Yu, F. Kagawa, S. Seki, M. Kubota, J. Masell, F. S. Yasin, K. Nakajima, M. Nakamura, M. Kawasaki, N. Nagaosa, and Y. Tokura, Nat. Commun. **12**, 5079 (2021).

[12] X. S. Wang, H. Y. Yuan, and X. R. Wang, Commun. Phys. **1**, 31 (2018).

[13] D. Amoroso, P. Barone, and S. Picozzi, Nat. Commun. **11**, 5784 (2020).

[14] M. Hoffmann, B. Zimmermann, G. P. Muller, D. Schurhoff, N. S. Kiselev, C. Melcher, and S. Blugel, Nat. Commun. **8**, 308 (2017).

[15] Y. Nagaosa and N. Tokura, Nat. Nanotechnol. **8**, 899 (2013).

[16] R. Ozawa, S. Hayami, and Y. Motome, Phys. Rev. Lett. **118**, 147205 (2017).

[17] X. Yao and S. Dong, Phys. Rev. B **105**, 014444 (2022).

[18] X. Yao, D. Hu, and S. Dong, iScience **26**, 106311 (2023).

[19] Z. Shen, C. Song, Y. Xue, Z. Wu, J. Wang, and Z. Zhong, Phys. Rev. B **106**, 094403 (2022).

[20] Z. W. Zhong Shen, Y. Xue, and C. Song, Appl. Phys. Lett. **121**, 202402 (2022).

[21] W. Sun, W. Wang, H. Li, G. Zhang, D. Chen, J. Wang, and Z. Cheng, Nat. Commun. **11**, 5930 (2020).

[22] C. Xu, P. Chen, H. Tan, Y. Yang, H. Xiang, and L. Bellaiche, Phys. Rev. Lett. **125**, 037203 (2020).

[23] Y. Wang, S. Dong, and X. Yao, Physica E **153**, 115776 (2023).

[24] I. Dzyaloshinsky, J. Phys. Chem. Solids **4**, 241 (1958).

[25] T. Moriya, Phys. Rev. **120**, 91 (1960).

[26] S. Zhang and Z. Li, Phys. Rev. Lett. **93**, 127204 (2004).

[27] J. Slonczewski, J. Magn. Magn. Mater. **159**, L1 (1996).

[28] L. Berger, Phys. Rev. B **54**, 9353 (1996).

[29] L. Kong and J. Zang, Phys. Rev. Lett. **111**, 067203 (2013).

[30] J. Wang, M. Strungaru, S. Ruta, A. Meo, Y. Zhou, A. Deak, L. Szunyogh, P.-I. Gavriloaea, R. Moreno, O. Chubykalo-Fesenko, J. Wu, Y. Xu, R. F. L. Evans, and R. W. Chantrell, Phys. Rev. B **104**, 054420 (2021).

[31] R. Hertel, S. Gliga, M. Fähnle, and C. M. Schneider, Phys. Rev. Lett. **98**, 117201 (2007).

[32] C. Moutafis, S. Komineas, and J. A. C. Bland, Phys. Rev. B **79**, 224429 (2009).

[33] Y. Nii, T. Nakajima, A. Kikkawa, Y. Yamasaki, K. Ohishi, J. Suzuki, Y. Taguchi, T. Arima, Y. Tokura, and Y. Iwasa, Nat. Commun. **6**, 8539 (2015).

[34] L. Jiang, C. Huang, Y. Zhu, Y. Pan, J. Fan, K. Zhang, C. Ma, D. Shi, and H. Zhang, iScience **25**, 104039 (2022).

[35] Q. Cui, Y. Zhu, J. Jiang, J. Liang, D. Yu, P. Cui, and H. Yang, Phys. Rev. Res. **3**, 043011 (2021).

[36] F. Matsukura, Y. Tokura, and H. Ohno, Nat. Nanotechnol. **10**, 209 (2015).

[37] P.-J. Hsu, A. Kubetzka, A. Finco, N. Romming, K. von Bergmann, and R. Wiesendanger, Nat. Nanotechnol. **12**, 123 (2017).

[38] G. Kresse and J. Furthmuller, Phys. Rev. B **54**, 11169 (1996).

[39] A. Togo and I. Tanaka, Scr. Mater. **108**, 1 (2015).

[40] A. Togo, F. Oba, and I. Tanaka, Phys. Rev. B **78**, 134106 (2008).

[41] K. Momma and F. Izumi, J. Appl. Crystallogr. **44**, 1272 (2011).

[42] L. D. Landau and E. M. Lifshitz, Phys. Z. Sowjetunion **8**, 51 (1935).

[43] T. L. Gilbert, IEEE Trans. Magn. **40**, 3443 (2004).

[44] G. P. Müller, M. Hoffmann, C. Dißelkamp, D. Schürhoff, S. Mavros, M. Sallermann, N. S. Kiselev, H. Jónsson, and S. Blügel, Phys. Rev. B **99**, 224414 (2019).

[45] See Supplemental Material at http://link.aps.org/supplemental/10.1103/PhysRevB.108.L140412 for (a) calculation details; (b) details of the crystal structure; (c) the calculations of magnetic parameters; (d) the underlying mechanisms of the L-dependent MAE; (e) the specific values of magnetic parameters; and (f) the stability of skyrmions and bimerons under different temperatures, which includes Refs. [80–82].

[46] W. Ding, J. Zhu, Z. Wang, Y. Gao, D. Xiao, Y. Gu, Z. Zhang, and W. Zhu, Nat. Commun. **8**, 14956 (2017).

[47] Y. Zhou, D. Wu, Y. Zhu, Y. Cho, Q. He, X. Yang, K. Herrera, Z. Chu, Y. Han, M. C. Downer, H. Peng, and K. Lai, Nano Lett. **17**, 5508 (2017).

[48] S. Yuan, W. F. Io, J. Mao, Y. Chen, X. Luo, and J. Hao, ACS Appl. Nano Mater. **3**, 11979 (2020).

[49] H. Yang, M. Xiao, Y. Cui, L. Pan, K. Zhao, and Z. Wei, Sci. China Inf. Sci. **62**, 220404 (2019).

[50] L. Zhang, X. Huang, H. Dai, M. Wang, H. Cheng, L. Tong, Z. Li, X. Han, X. Wang, L. Ye, and J. Han, Adv. Mater. **32**, e2002032 (2020).

[51] N.-S. Liu, C. Wang, and W. Ji, Acta Phys. Sin. **71**, 127504 (2022).

[52] C. Wang, X. Zhou, L. Zhou, Y. Pan, Z.-Y. Lu, X. Wan, X. Wang, and W. Ji, Phys. Rev. B **102**, 020402(R) (2020).

[53] H. W. N. D. Mermin, Phys. Rev. Lett. **17**, 1133 (1966).

[54] S. Jenkins, L. Rozsa, U. Atxitia, R. F. L. Evans, K. S. Novoselov, and E. J. G. Santos, Nat. Commun. **13**, 6917 (2022).

[55] J. Lado and J. L. Fernández-Rossier, 2D Mater. **4**, 035002 (2017).

[56] X. Zhang, Q. Lu, W. Liu, W. Niu, J. Sun, J. Cook, M. Vaninger, P. F. Miceli, D. J. Singh, S. W. Lian, T. R. Chang, X. He, J. Du, L. He, R. Zhang, G. Bian, and Y. Xu, Nat. Commun. **12**, 2492 (2021).

[57] J. Liu, M. Shi, J. Lu, and M. P. Anantram, Phys. Rev. B **97**, 054416 (2018).

[58] D. S. Wang, R. Wu, and A. J. Freeman, Phys. Rev. B **47**, 14932 (1993).

[59] B. S. Yang, J. Zhang, L. N. Jiang, W. Z. Chen, P. Tang, X.-G. Zhang, Y. Yan, and X. F. Han, Phys. Rev. B **95**, 174424 (2017).

[60] H. Yang, G. Chen, A. A. C. Cotta, A. T. N'Diaye, S. A. Nikolaev, E. A. Soares, W. A. A. Macedo, K. Liu, A. K. Schmid, A. Fert, and M. Chshiev, Nat. Mater. **17**, 605 (2018).

[61] L. Wang, Q. Feng, Y. Kim, R. Kim, K. H. Lee, S. D. Pollard, Y. J. Shin, H. Zhou, W. Peng, D. Lee, W. Meng, H. Yang, J. H. Han, M. Kim, Q. Lu, and T. W. Noh, Nat. Mater. **17**, 1087 (2018).

[62] K. Zeissler, S. Finizio, C. Barton, A. J. Huxtable, J. Massey, J. Raabe, A. V. Sadovnikov, S. A. Nikitov, R. Brearton, T. Hesjedal, G. van der Laan, M. C. Rosamond, E. H. Linfield, G. Burnell, and C. H. Marrows, Nat. Commun. **11**, 428 (2020).

[63] H. Yang, A. Thiaville, S. Rohart, A. Fert, and M. Chshiev, Phys. Rev. Lett. **115**, 267210 (2015).

[64] Y. Ga, Q. Cui, Y. Zhu, D. Yu, L. Wang, J. Liang, and H. Yang, npj Comput. Mater. **8**, 128 (2022).

[65] J. Liang, W. Wang, H. Du, A. Hallal, K. Garcia, M. Chshiev, A. Fert, and H. Yang, Phys. Rev. B **101**, 184401 (2020).

[66] J. H. Yang, Z. L. Li, X. Z. Lu, M. H. Whangbo, S. H. Wei, X. G. Gong, and H. J. Xiang, Phys. Rev. Lett. **109**, 107203 (2012).

[67] W. Du, K. Dou, Z. He, Y. Dai, B. Huang, and Y. Ma, Nano Lett. **22**, 3440 (2022).

[68] Q. Cui, J. Liang, Z. Shao, P. Cui, and H. Yang, Phys. Rev. B **102**, 094425 (2020).

[69] A. Fert and P. M. Levy, Phys. Rev. Lett. **44**, 1538 (1980).

[70] W.-J. Li, Y. Guang, G.-Q. Yu, C.-H. Wan, J.-F. Feng, and X.-F. Han, Acta Phys. Sin. **67**, 131204 (2018).

[71] Y.-Z. Liu and J. Zang, Acta Phys. Sin. **67**, 131201 (2018).

[72] J. Jiang, X. Liu, R. Li, and W. Mi, Appl. Phys. Lett. **119**, 072401 (2021).

[73] W. Legrand, D. Maccariello, F. Ajejas, S. Collin, A. Vecchiola, K. Bouzehouane, N. Reyren, V. Cros, and A. Fert, Nat. Mater. **19**, 34 (2020).

[74] B. Göbel, I. Mertig, and O. A. Tretiakov, Phys. Rep. **895**, 1 (2021).

[75] B. Gobel, A. Mook, J. Henk, I. Mertig, and O. A. Tretiakov, Phys. Rev. B **99**, 060407(R) (2019).

[76] D. Li, S. Haldar, and S. Heinze, Nano Lett. **22**, 7706 (2022).

[77] B. Huang, G. Clark, E. Navarro-Moratalla, D. R. Klein, R. Cheng, K. L. Seyler, D. Zhong, E. Schmidgall, M. A. McGuire, D. H. Cobden, W. Yao, D. Xiao, P. Jarillo-Herrero, and X. Xu, Nature (London) **546**, 270 (2017).

[78] Q. Cui, J. Liang, B. Yang, Z. Wang, P. Li, P. Cui, and H. Yang, Phys. Rev. B **101**, 214439 (2020).

[79] R. Zarzuela, V. K. Bharadwaj, K.-W. Kim, J. Sinova, and K. Everschor-Sitte, Phys. Rev. B **101**, 054405 (2020).

[80] M. Pizzochero and O. V. Yazyev, J. Phys. Chem. C **124**, 7585 (2020).

[81] J. P. Perdew, K. Burke, and M. Ernzerhof, Phys. Rev. Lett. **77**, 3865 (1996).

[82] Z. Hao, H. Li, S. Zhang, X. Li, G. Lin, X. Luo, Y. Sun, Z. Liu, and Y. Wang, Sci. Bull. **63**, 825 (2018).